Novel fluorescent cyclic nucleotide derivatives to study CNG and HCN

channel function

Maik Otte^{1,§}, Andrea Schweinitz^{1,§}, Marco Lelle^{1,§}, Susanne Thon¹ Uta Enke¹, Sezin Yüksel¹, Ralf

Schmauder¹, Michele Bonus², Holger Gohlke^{2,3}, Klaus Benndorf^{1,*}

¹Institut für Physiologie II, Universitätsklinikum Jena, Friedrich-Schiller-Universität Jena, 07740 Jena,

Germany.

²Institut für Pharmazeutische und Medizinische Chemie, Heinrich-Heine-Universität Düsseldorf, 40225

Düsseldorf, Germany.

³John von Neumann Institute for Computing (NIC), Jülich Supercomputing Centre (JSC) & Institute for

Complex Systems - Structural Biochemistry (ICS 6), Forschungszentrum Jülich GmbH, Jülich,

Germany.

Running Title: Fluorescent cGMP and cAMP derivatives

* Address correspondence to:

Prof. Dr. Klaus Benndorf, Friedrich Schiller University Jena, Jena University Hospital, Institute of

Physiology II, Kollegiengasse 9, 07743 Jena

phone: +49 3641 934350

fax: +49 3641 933202

e-mail: Klaus.Benndorf@med.uni-jena.de

§contributed equally to this work

1

ABSTRACT

A highly specific molecular interaction of diffusible ligands with their receptors belongs to the key processes in cellular signaling. Because an appropriate method to monitor the unitary binding events is still missing, most of our present knowledge is based on ensemble signals recorded from a big number of receptors, such as ion currents or fluorescence changes of suitably labeled receptors, and reasoning from these data to the binding process itself. To study the binding process itself, appropriately tagged ligands are required which fully activate the receptors and report the binding at the same time. Herein, we tailored a series of 18 novel fluorescent cyclic nucleotide derivatives by attaching six different dyes via different alkyl linkers to the 8-position of the purine ring of cGMP or cAMP. The biological activity was determined in inside-out macro-patches containing either homotetrameric (CNGA2), heterotetrameric (CNGA2:CNGA4:CNGB1b) or hyperpolarization-activated cyclic nucleotide-modulated (HCN2) channels. All these novel fluorescent ligands are efficient to activate the channels and the potency of most of them significantly exceeded that of the natural cyclic nucleotides cGMP or cAMP. Moreover, some of them showed an enhanced brightness when bound to the channels. The best of our derivatives bear great potential to systematically analyze the activation mechanism in CNG and HCN channels, at both the level of ensemble and single-molecule analyses.

INTRODUCTION

Cyclic nucleotide–gated (CNG) channels, generating receptor potentials in olfactory sensory neurons and photoreceptors (3, 4), are activated by the intracellular binding of the second messengers cyclic guanosine-3',5'-monophosphate (cGMP) or cyclic adenosine-3',5'-monophosphate (cAMP). CNG channels are tetrameric non-specific cation channels and, structurally, they belong to the superfamily of six-transmembrane domain voltage-gated channels (5). Native mammalian olfactory CNG channels are built of three different but homologue subunits, 2×CNGA2, CNGB4 and CNGB1b. Each of these subunits binds a cyclic nucleotide and actively contributes to channel activation (6, 7). At heterologous expression CNGA2 subunits can also form functional homotetrameric channels (3). Recently, for homologue TAX-4 channels of *Caenorhabditis elegans*, a full channel structure at 3.5 Å resolution has been determined (1).

Hyperpolarization-activated cyclic nucleotide-modulated (HCN) channels (1, 8-13) are structurally related to CNG channels. These channels generate electrical rhythmicity in specialized brain neurons and cardiomyocytes (14). In contrast to CNG channels, HCN channels have to be primarily activated by sufficiently hyperpolarizing membrane voltage, and cyclic nucleotides only enhance activation.

Besides the native agonists cGMP and cAMP, also multiple derivatives of them have been synthesized and tested on their ability to activate CNG or HCN channels (15-19) or to bind to isolated CNBDs of HCN channels (13, 20, 21). Among these compounds were also several that contained a fluorophore at the end of the 8-substituent, including fluorescein (17, 20, 22), NBD (18) and DY547 introduced by our group (6, 23-25). We recently extended the list of 8-thio-substituted compounds by systematically introducing chains of different length and degree of hydrophobicity. Previous studies showed that for a bound cyclic nucleotide there is sizeable space at the entrance of the binding pocket (15, 26).

Despite there has been notable progress in our understanding of CNG and HCN channel activation, many questions remain unanswered. It is particularly desirable to study the processes of ligand binding and unbinding and their relation to channel activation and deactivation at both faster time scale and also at the single-molecule level. For these experimental strategies novel fluorescent cyclic nucleotides with advanced properties are required. Such ligands should have a suitable fluorophore emitting bright fluorescence when bound to the binding site, while being fully efficient and, at the same time, highly potent to activate the channels at reasonably low concentrations, allowing thus to minimize background fluorescence.

Herein, we synthesized a series of novel fluorescent cyclic nucleotide derivatives which combine these properties to different degrees and, by employing the patch-clamp technique and confocal patch-clamp fluorometry, we quantified channel activation and ligand binding in homotetrameric and heterotetrameric channels in detail. Concerning the potency, the cGMP derivatives generated a similar pattern for homo- and heterotetrameric channels. The cAMP derivatives also generated a similar pattern for homo- and heterotetrameric channels, which was, however, different from that of cGMP. Moreover, for six selected cAMP derivatives the activating effect was also quantified on homotetrameric HCN2 channels. Together, these novel compounds are new tools to study the specific interactions of cyclic

nucleotides with CNG and HCN channels, and the best of these compounds bear potential to unravel the process of ligand binding by optical approaches, ultimately down to the single-molecule level.

Materials and Methods

Synthesis of the fluorescent cNMP derivatives

The derivatives $\mathbf{3}_G$ and $\mathbf{3}_A$ were obtained from BIOLOG (Bremen, Germany). The syntheses of the other used compounds are described in detail in Supplemental Methods. The compounds were synthesized from the corresponding 8-substituted cNMP derivatives, bearing an amino group as described in (26), by standard NHS-ester coupling of the fluorophore.

Molecular Biology

The subunits CNGA2 (accession No. AF126808), CNGA4 (accession No. U12623) and CNGB1b (accession No. AF068572) of rat olfactory channels as well as mouse HCN2 channels (NM008226) were subcloned behind the T7 promoter of pGEMHEnew. The corresponding cRNAs were generated by using the mMESSAGE mMACHINE T7 Kit (Ambion, Austin, TX).

Functional expression in Xenopus oocytes

Oocytes of *Xenopus laevis* were obtained either from Ecocyte (Castrop-Rauxel, Germany) or surgically from female adults under anesthesia (0.3 % 3-aminobenzoic acid ethyl ester). The procedures had approval from the authorized animal ethical committee of the Friedrich Schiller University Jena. The methods were performed according to the approved guidelines.

The oocytes were incubated for 105 min in Ca²⁺-free Barth's solution containing collagenase A (3 mg/ml; Roche, Grenzach-Wyhlen, Germany) containing (in mM) 82.5 NaCl, 2 KCl, 1 MgCl₂, 5 Hepes, pH 7.4. Oocytes at stages IV and V were injected with 15 – 35 ng cRNA encoding either CNGA2, CNGA2:CNGA4:CNGB1b (2:1:1 ratio) or HCN2 channels either manually or by means of an injection robot (RoboInject®, Multi Channel Systems, Reutlingen, Germany). The injected oocytes were incubated at 18°C for up to 6 days in Barth's solution containing (in mM) 84 NaCl, 1 KCl, 2.4 NaHCO₃, 0.82 MgSO₄, 0.41 CaCl₂, 0.33 Ca(NO₃)₂, 7.5 TRIS, cefuroxime (4.0 μg×ml⁻¹), and penicillin/streptomycin (100 μg/ml), pH 7.4.

Electrophysiology

Macroscopic currents were recorded in inside-out patches of the oocytes expressing the desired channels by using standard patch-clamp techniques (27). The patch pipettes were pulled from quartz tubing (P-2000, Sutter Instrument, Novato, USA) with an outer and inner diameter of 1.0 and 0.7 mm (VITROCOM, New Jersey, USA). The corresponding pipette resistance was 0.9 - 2.3 MΩ. The bath and pipette solution contained (in mM): 150 KCl, 1 EGTA, 5 Hepes (pH 7.4 with KOH) for CNG channel measurements. For HCN channel measurements the bath solution contained 100 mM KCl, 10 mM EGTA, 10 mM HEPES (pH 7.2) and 120 mM KCl, 10 mM HEPES, and 1.0 mM CaCl₂ (pH 7.2) in the pipette. All recordings were performed at room temperature by using an Axopatch 200B amplifier (Axon Instruments, Foster City, CA). Electrophysiology was controlled by the LIH8+8 data acquisition interface and the Patchmaster-software (HEKA Elektronik Dr. Schulze GmbH, Lambrecht, Germany). The sampling rate was 5 kHz and the filter implemented in the amplifier (4-pole Bessel) was set to 2 kHz. Measurements in HCN2 channels were started 3.5 min after patch excision to minimize rundown phenomena (9, 19, 28). The solutions with the ligand concentrations to be tested were applied via a multi-barrel device to the patches with a flow rate of 0.8 to 1.2 ml/min. The concentration of all ligand stock solutions were verified by UV spectroscopy.

Confocal patch-clamp fluorometry

The binding of fluorescent ligands and the ionic current in macropatches were measured simultaneously by confocal patch-clamp fluorometry (cPCF) as described (23, 24). The patch pipettes were pulled from borosilicate glass tubing with an outer and inner diameter of 2.0 and 1.0 mm (Hilgenberg GmbH, Malsfeld, Germany). The pipette resistance was 0.7-1.2 M Ω . The bath and pipette solution contained (in mM): 150 KCl, 1 EGTA, 5 Hepes (pH 7.4 with KOH). Recordings were performed with an LSM 710 confocal microscope equipped with a 40x/1.2 water-immersion objective (Zeiss, Jena, Germany) and were triggered by the ISO3 software (MFK, Niedernhausen, Germany). To distinguish the fluorescence of the unbound fluorescent ligands from that of the bound fluorescent ligands, a second dye, DY647 (Dyomics, Jena, Germany), was added to the bath solution at a concentration of 5 μ M. The fluorescent ligands and DY647 were excited at 543 nm and 633 nm, respectively and detection bands

of 546-635 nm and 637-759 nm were selected. The fluorescence intensity from the reference dye was scaled on the fluorescence intensity of the free ligand in the bath and the pipette interior. In the patch dome building the difference between both provided the surplus of the green fluorescence which was used to quantify the portion of bound ligands (23). The actual relative fluorescence, F, was normalized in each patch with respect to the fluorescence F_{max} at a saturating concentration of the same fluorescent ligand.

Fitting steady-state concentration-activation and concentration-binding relationships

Concentration-activation relationships were fitted with the Igor software® by

$$I/I_{\text{max}} = 1/[1 + (EC_{50}/[CN])^{Ha}]. \tag{1}$$

I is the actual current amplitude and I_{max} the maximum current amplitude at saturating cGMP (100 μ M) or cAMP (500 μ M) concentration. EC_{50} is the ligand concentration generating the half maximum current and H_a the respective Hill coefficient. [CN] is the actual concentration of the cyclic nucleotide to be tested.

Accordingly, concentration-binding relationships were fitted with the same software by

$$F/F_{\text{max}} = 1/[1 + (BC_{50}/[\text{CN}])^{Hb}].$$
 (2)

F is the actual relative fluorescence intensity and F_{max} the maximum relative fluorescence intensity at a saturating concentration of the same fluorescent ligand. BC_{50} is the ligand concentration generating half maximum binding, H_{b} the respective Hill coefficient and [CN] the actual concentration of the cyclic nucleotide to be tested.

Errors are given as mean \pm s.e.m.

Molecular docking

The homotetrameric rat CNGA2 structure (UniProt accession ID: Q00195) was generated by homology modeling, using the 3.5 Å cryo-EM structure of the cyclic nucleotide-gated cation channel TAX-4 (PDB ID: 5H3O) as a template (1). The modeling was carried out by the SWISS-MODEL server (29) based on a target-template alignment with a sequence identity of 54.5% and coverage of 69%, and using

residues 127-583 of a channel subunit. The quality of the model was validated by the MolProbity server (30), yielding an overall MolProbity score of 1.42.

Molecular docking of **8**_G to the rat CNGA2 channel CNBD was performed using AutoDockTools 4.2 (ADT 4.2). Since a correct assignment of the partial atomic charges was not possible with ADT 4.2, the point charges were derived using quantum mechanical calculations. First, a gas-phase geometry optimization of **8**_G was carried out at the HF/6-31G(d) level using GAUSSIAN 09, Revision B.01 (31). Subsequently, the molecular electrostatic potential (MEP) was computed at the same level of theory using the R.E.D. server (32). To obtain the atomic charges that best reproduce the MEP, the RESP procedure (33) with two fitting stages (hyperbolic constraint values: 0.0005/0.001) was employed (34, 35). We obtained different stereoisomers of the dye in the *cis* (*SR*, *RS*) and *trans* configuration (*SS*, *RR*). The computation yielded differences in the internal energy of roughly 5 kcal/mol. The favored stereoisomer is *cis* and, therefore, the RS configuration was used for the molecular docking.

The docking grid in a CNGA2 monomer was defined by superimposition of the cGMP-bound TAX-4 cryo-EM structure (chain A) onto chain A of the CNGA2 homology model. The coordinates of cGMP in the TAX-4 structure were used as coordinates for the center of the docking grid in CNGA2. The X,Y,Z dimensions of the box were set to 60x60x60 with a spacing of 0.375 Å. There were no defined constraints, rotatable groups, or excluded volumes. Docking was performed using the Lamarckian genetic algorithm (36) with a maximum of 25,000,000 energy evaluations and a maximum of 27,000 generations. **8**_G was docked in three independent experiments, using 30-50 genetic algorithm runs each and identifying 12 poses with comparable native binding poses. Among these the largest cluster contained five poses, and the best thereof is shown in Figure 7 with a binding energy of -5.81 kcal/mol.

Results

Effects of fluorescent cGMP and cAMP derivatives on EC₅₀ in CNGA2 and

CNGA2:CNGA4:CNGB1b channels

The activating effects of cGMP $(\mathbf{1}_G)$ and cAMP $(\mathbf{1}_A)$ and their derivatives were determined by voltage pulses to -10 and +10 mV. For determining equilibrium activation at a given concentration, the amplitude of the late current at +10 mV, I, was evaluated (Fig. 1A). All current amplitudes I were related to the current amplitude at the respective saturating cGMP and cAMP concentration of 100 µM and 500 μ M, yielding the relative current amplitudes I/I_{cGMP} and I/I_{cAMP} . The plots of I/I_{cGMP} or I/I_{cAMP} versus the concentration of the actual cyclic nucleotide were fitted with the Hill equation (equation 1; Fig. 1B) vielding the respective EC₅₀ and H_a values. Referring to our previous results we introduced different hydrophobic alkyl chains to the 8-position of purine ring of the cyclic nucleotides (Otte et al., 2018) and coupled to these linkers the dyes DY547, DY547P1, Cy3Me, Cy3B, DY557 and PDI (Fig. 2; Supplemental Methods). The resulting fluorescent cyclic nucleotide derivatives exerted characteristic and systematic effects on both CNGA2 and CNGA2:CNGA4:CNGB1b channels (Fig. 1C-F; Table S1). Consider the effects of the cGMP derivatives on EC_{50} for both types of channels. For the first three of the dyes in Figure 1C,D and DY557 both an ethyl and a hexyl linker were inserted. For PDI only a hexyl linker was inserted whereas for Cy3B a hexyl and a decyl linker were inserted to reach comparable linker lengths between ligand and fluorophore. In total this resulted in eleven fluorescent derivatives (2_G-12_G) (Table 1). All of these fluorescent cyclic nucleotides were full agonists. The EC_{50} values differed notably among the eleven derivatives (Fig. 1C,D; Table S1A,B).

Comparison of the effects of the cGMP derivatives on homotetrameric CNGA2 channels shows that all thio-substituted derivatives have a higher apparent affinity than natural cGMP (Fig. 1C). This corresponds to previous reports demonstrating that various thio-substitutions in 8-position enhance the apparent affinity to CNG channels (17, 37) and matches also our own observations that extension of a thio-substituted alkyl chain in 8-position increases the apparent affinity (26). The derivatives $\mathbf{4}_G$ and $\mathbf{6}_G$, both containing a short linker, were similar to native cGMP. In the case of the conventional cyanine-like dyes a longer linker enhances the apparent affinity notably $(\mathbf{2}_{G}-\mathbf{3}_{G}, \mathbf{4}_{G}-\mathbf{5}_{G}, \mathbf{6}_{G}-\mathbf{7}_{G})$ whereas in case of cGMP-derivatives (\mathbf{X}_G)

No. of compound	Linker type	Linker Structures at 8-position (R)	Amount of atoms	Dye
1 _{A/G}	-	_H	-	-
2 _{A/G}	8-AET-	N-dye	8	-DY547
3 _{A/G}	8-AHT-	N-dye	12	
4 _{A/G}	8-AET-	N-dye	10	-DY547P1
5 _{A/G}	8-AHT-	N-dye	14	
6 _{A/G}	8-AET-	N-dye	10	Су3Ме
7 _{A/G}	8-AHT-	N-dye	14	
8 _{A/G}	8-AHT-	N-dye	10	-Су3В
9 _{A/G}	8-ADT-	N-dye	14	
10 _{A/G}	8-AET-	N-dye	12	-DY557
11 _{A/G}	8-AHT-	N-dye	16	
12 _G	8-AHT-	N-dye	11	–PDI

Table 1. Overview of fluorescent cyclic-nucleotide derivatives used in the experiments. cNMP is either cGMP (XG) or cAMP (XA); 8-AET: 8-((2-aminoethyl)thio)-; 8-AHT: 8-((6-aminohexyl)thio)-; 8-ADT: 8-((10-aminodecyl)thio)-linker. For dye structures see Figure 2.

two other pairs with the same dye and differently long linker the apparent affinity with the longer linker

was either similar ($\mathbf{8}_{G}$ - $\mathbf{9}_{G}$) or even lower ($\mathbf{10}_{G}$ - $\mathbf{11}_{G}$). This suggests that a longer linker alone does not necessarily increase the apparent affinity. Thus, the dye moieties themselves, and eventually the location of the amide group, presumably exert additional effects on the binding. Together, the best apparent affinity was obtained with $\mathbf{3}_{G}$ which was 18.8 times higher than with cGMP. However, gradually increased apparent affinities were also obtained with other derivatives.

When considering the effects of the same cGMP derivatives (2_{G} - 12_{G}) on heterotetrameric CNGA2:CNGA4:CNGB1b channels, it is evident that despite the replacement of two CNGA2 subunits by one CNGA4 and one CNGB1b subunit the compounds exert a closely similar pattern of effects on the channels (Fig. 1D). Because both the CNGA4 and CNGB1b subunit contributes to channel activation themselves by binding a ligand (6, 7), it is likely that all tested cGMP derivatives act in a similar manner on all three types of subunits. Among all derivatives, the best fluorescent ligand 3_{G} had a 6.2 times higher apparent affinity compared to cGMP (1_{G}). The similarity in the degree of increase of the apparent affinity is further outlined by plotting the EC_{50} values for heterotetrameric channels versus the EC_{50} values for homotetrameric channels (Fig. 3). Though there is a slightly higher apparent affinity of the compounds for homotetrameric channels, all cGMP derivatives group near the dashed line, which indicates a theoretical equal effect on both types of channels.

Next, the effects of ten respective cAMP derivatives ($\mathbf{2}_{A}$ - $\mathbf{11}_{A}$) on EC_{50} are considered (Fig 1E,F). A respective compound $\mathbf{12}_{A}$ was not synthesized because of a questionable reversibility of the effects of $\mathbf{12}_{G}$ in CNG channels. When considering the effects on homotetrameric CNGA2 channels, three compounds $\mathbf{4}_{A}$, $\mathbf{10}_{A}$, and $\mathbf{11}_{A}$ produced an EC_{50} value similar to that of cAMP ($\mathbf{1}_{A}$) ($EC_{50} = 52.8 \, \mu M$), one compound ($\mathbf{2}_{A}$) even decreased the apparent affinity with respect to cAMP whereas five derivatives ($\mathbf{3}_{A}$, $\mathbf{5}_{A}$, $\mathbf{7}_{A}$, $\mathbf{8}_{A}$, $\mathbf{9}_{A}$) significantly increased the apparent affinity (Fig. 1E). In the case of $\mathbf{8}_{A}$ and $\mathbf{9}_{A}$ the gain in apparent affinity with respect to cAMP was 13.2 and 34.1 fold, respectively. Pairs of derivatives with the same fluorophore had generally a higher apparent affinity in the case of the hexyl than of the ethyl linker with the only exception being the DY557 derivatives ($\mathbf{10}_{A}$ - $\mathbf{11}_{A}$) for which the apparent affinity was indistinguishable. Because the ethyl linker in $\mathbf{10}_{A}$ has already a length of 12 atoms, it is

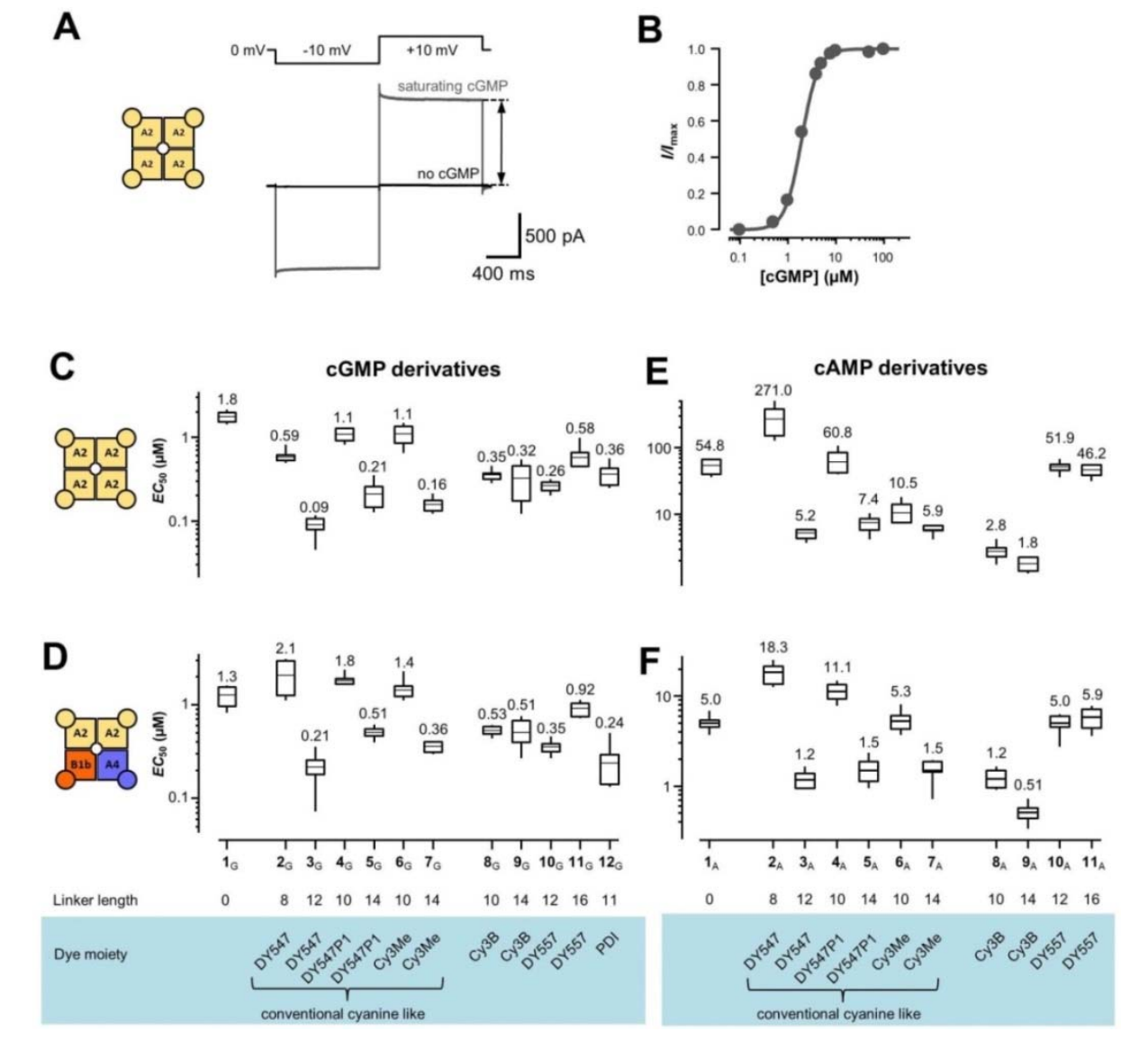


Figure 1. Determination of the effects of the cyclic nucleotides and its derivatives on EC_{50} . (A) Example of a current response generated by CNGA2 channels to cGMP ($\mathbf{1}_{G}$) according to the indicated voltage protocol. (B) Equilibrium concentration-activation relationship. The data points were obtained from one patch. The curve was determined by fitting equation 1 yielding EC_{50} = 1.9 μ M H_{a} = 2.52. (C) Box plots of EC_{50} values for CNGA2 channels and cGMP derivatives. Displayed are the means as a horizontal line within each box, the boxes as 25th and 75th percentiles and the whiskers as 10th and 90th percentiles of the data. The numeric mean values are indicated above each box. The indicated linker length count from the sulfur to the last linker atom. For structures of the dye moieties see Figure 2. (D-F) analogue to C. (D) CNGA2:CNGA4:CNGB1b channels and cGMP derivatives. (E) CNGA2 channels and cAMP derivatives.

likely that a further extension to 16 atoms in **11**_A does not produce additional benefit for binding. Also these compounds were full agonists apart from **6**_A which activated CNGA2 and CNGA2:CNGA4:CNGB1b channels at saturating concentrations to only 89% and 82%, respectively (Table S1C,D). On CNGA2:CNGA4:CNGB1b the best compound was again **9**_A. The overall pattern of

the compounds differs from that of the cGMP derivatives (compare Fig. 1E with Fig. 1C), reflecting specificities arising from the different cyclic nucleotides.

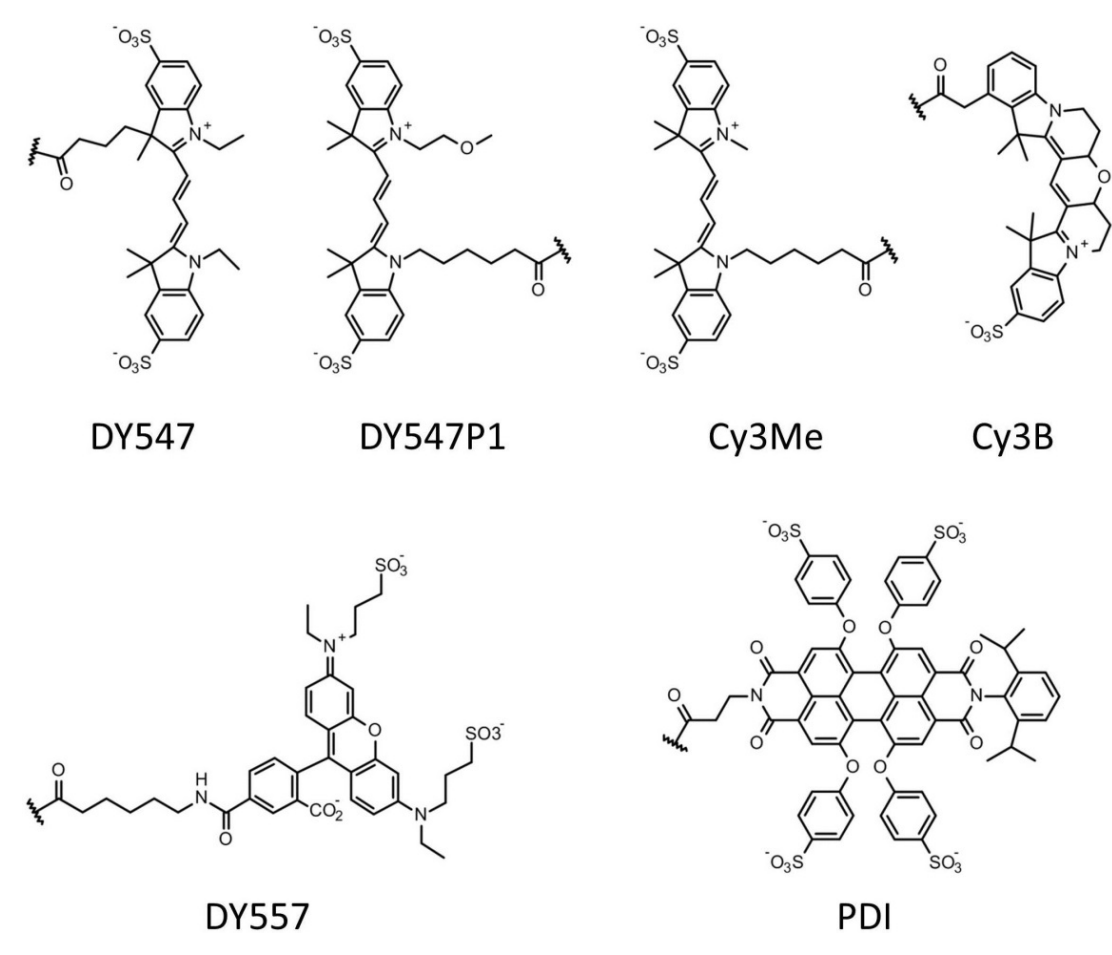


Figure 2. Structures of the dyes used in the fluorescent derivatives. The dyes were attached to linkers which were coupled to the 8-position of the cyclic nucleotides (c.f. Table 1).

When comparing the effects of the cAMP derivatives on heterotetrameric CNGA2:CNGA4:CNGB1b channels (Fig. 1F) with those on homotetrameric CNGA2 channels (Fig. 1E), the pattern of the effects is roughly preserved with a tendency of stronger effects in homo- than in heterotetrameric channels, while all absolute EC_{50} values are significantly smaller in the heterotetrameric channels. The relation between the effects on the apparent affinity in homo- and heterotetrameric channels is again illustrated by Fig. 3. Similar to the cGMP derivatives there is approximately a direct proportionality for the cAMP derivatives concerning their effects on homo- and heterotetrameric channels but, dissimilar to the cGMP derivatives, cAMP and its derivatives have a generally higher apparent affinity for hetero- than homotetrameric channels. It is noteworthy, however, that $\mathbf{9}_{A}$ is the fluorescent cAMP derivative with the highest apparent affinity reported for these channels so far.

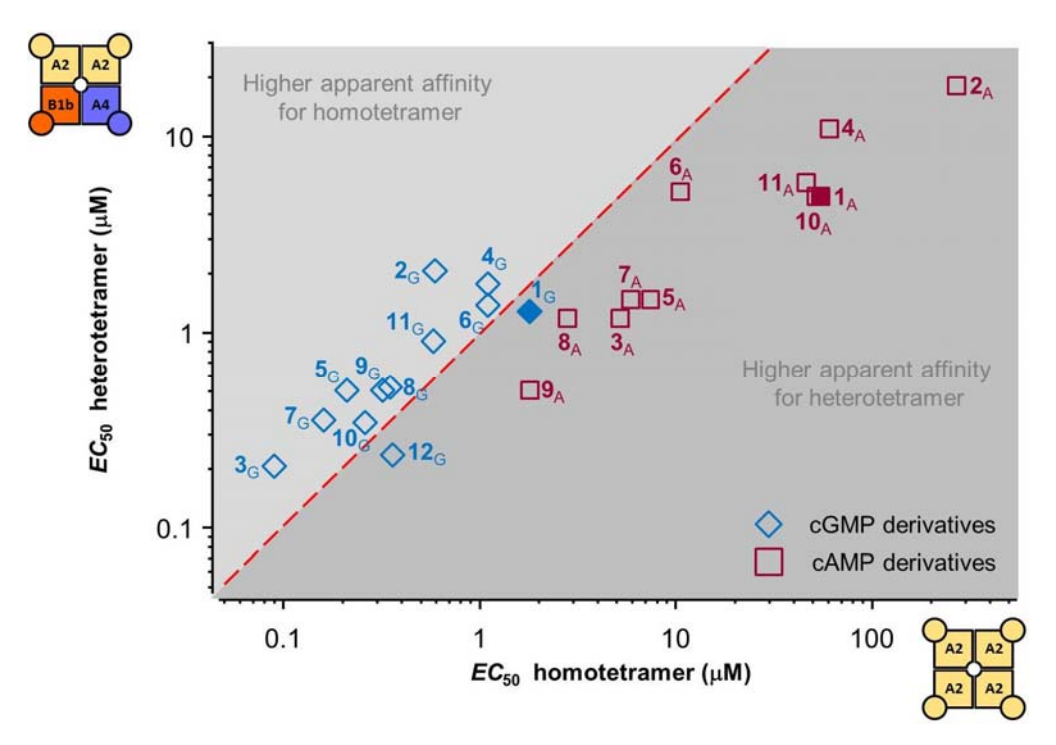


Figure 3. Potency of the fluorescent cyclic nucleotide derivatives in homo- and heterotetrameric CNG channels. Plotted are the EC_{50} values of heterotetrameric versus those of homotetrameric channels. The dashed red line indicates (theoretical) equal potency of the compounds for both types of channels. cAMP derivatives are more potent on heterotetrameric channels whereas cGMP derivatives are similarly potent on both channel types.

Effects of fluorescent cGMP and cAMP derivatives on the Hill coefficient H_a in CNGA2 and CNGA2:CNGA4:CNGB1b channels

Our screening analysis allowed us also to systematically compare the effects of the dyes and linkers on the Hill coefficients H_a determined by equation 1. With the natural cGMP ($\mathbf{1}_G$) H_a was closely similar in CNGA2 and CNGA2:CNGA4:CNGB1b channels (Table S1A,B). For the cGMP derivatives $\mathbf{2}_G$ - $\mathbf{1}\mathbf{1}_G$ with homotetrameric CNGA2 channels, however, H_a ranged from 2.5 to 3.7 whereas the respective values with heterotetrameric CNGA2:CNGA4:CNGB1b channels were on average smaller, ranging only from 1.5 to 2.6 (c.f. Table S1). If the Hill coefficient is taken as measure for the degree of cooperativity this suggests that the dye and linker moieties modulate the interaction of the subunits in heterotetrameric channels more than in homotetrameric channels. The derivative $\mathbf{12}_G$ is not considered here because of its poor reversibility. Notably, there was neither an obvious similarity in the pattern for the action of the derivatives in homo- and heterotetrameric channels nor an obvious correlation between H_a and EC_{50} . The situation with cAMP ($\mathbf{1}_A$) differs from that with cGMP ($\mathbf{1}_G$) in two aspects. First,the effects of the cAMP derivatives $\mathbf{2}_A$ - $\mathbf{11}_A$ on CNGA2 channels showed a systematic difference: In all pairs

with the same dyes ($\mathbf{2}_{A}$ - $\mathbf{3}_{A}$, $\mathbf{4}_{A}$ - $\mathbf{5}_{A}$, $\mathbf{6}_{A}$ - $\mathbf{7}_{A}$, $\mathbf{8}_{A}$ - $\mathbf{9}_{A}$, $\mathbf{10}_{A}$ - $\mathbf{11}_{A}$) the shorter linker caused a lower H_{a} than the longer linker (Fig. 4A), suggesting that the shorter linker disturbs to some extent the interaction of the subunits. In the case of CNGA2:CNGA4:CNGB1b channels this effect was found also for $\mathbf{2}_{A}$ - $\mathbf{3}_{A}$, $\mathbf{4}_{A}$ - $\mathbf{5}_{A}$ whereas for the other three derivative pairs such an effect could not be resolved (Fig. 4B).

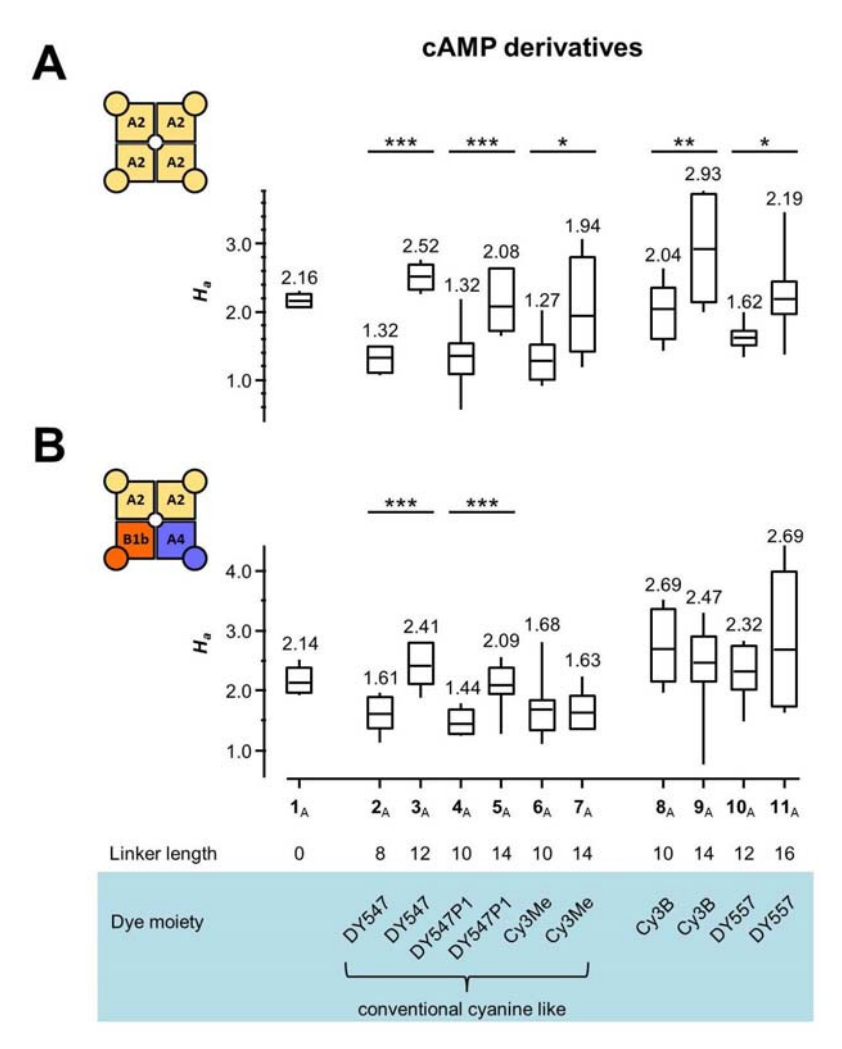


Figure 4. Determination of the effects of cAMP derivatives on H_a **in CNG channels.** (*A*) Box plots of H_a values for CNGA2 channels. For specification of boxes see Fig. 1. The numeric mean values are indicated above each box. (*B*) Box plots of H_a values for CNGA2:CNGA4:CNGB1b channels. Levels of significance: * P<0.1, ** P<0.05, *** P<0.01.

Concentration-binding relationships at equilibrium monitored by cPCF

The fluorescence of the dye moieties in bound derivatives were determined for the four dyes DY547, DY547P1, Cy3B and DY557 using $\mathbf{2}_G$, $\mathbf{4}_G$, $\mathbf{8}_G$ and $\mathbf{10}_G$, respectively. Cy3Me was not considered separately because its structure is closely similar to DY547P1, and PDI was excluded because its effects

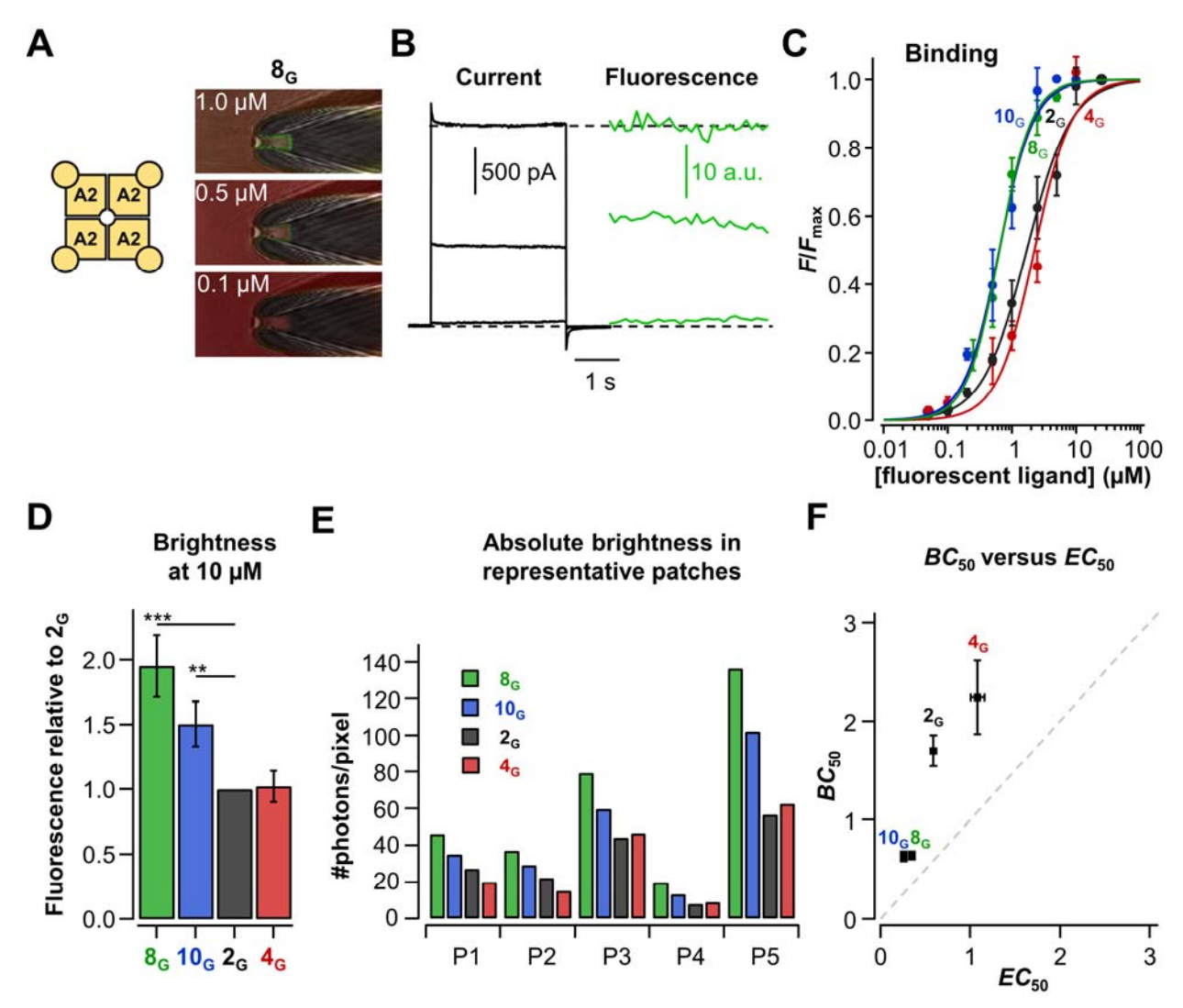


Figure 5. Ligand binding and activation in CNGA2 channels. The data were measured by confocal patch-clamp fluorometry (cPCF). (A) Images of an inside-out patch containing CNGA2 channels at three concentrations of 8_G. Green color shows specific ligand binding (see Materials and Methods) superimposed with the transmission micrograph. (B) Parallel recording of ligand binding, measured by the fluorescence intensity (green), and current activation, measured by a voltage pulse from 0 to 10 mV (black). (C) Concentration-binding relationships at equilibrium for 2_G , 4_G , 8_G and 10_G . The data points were fitted with equation 2 yielding the parameters half maximum binding, BC_{50} , and Hill coefficient for binding, H_b , respectively. **2**_G: BC_{50} =1.70 μ M, H_b =1.25; **4**_G: BC_{50} =2.24 μ M, H_b =1.49; **8**_G: BC_{50} =0.64 μ M, H_b =1.71; **10**_G: BC_{50} =0.63 μ M, H_b =1.60. (D) Brightness of four fluorescent derivatives bound to CNGA2 channels, each measured in five patches. The fluorescence intensities of 4_G, 8_G and 10_G were normalized with respect to that of 2_G . *** and ** indicate a significant difference with respect to 2_G when using a one-sample t-test with P<0.01 and P<0.05, respectively. (E) Comparison of the brightness, indicated by the number of photons per pixel for five individual patches at the 10 µM, a saturating concentration for all derivatives. The number of photons per pixel was estimated from arbitrary units by (signal/standard deviation)² using a non-fluctuating sample (Chroma-slides 92001). (F) Plot of BC_{50} versus EC_{50} for $\mathbf{2}_{G}$, $\mathbf{4}_{G}$, $\mathbf{8}_{G}$ and $\mathbf{10}_{G}$. The dashed line indicates a slope of one.

were only poorly reversible. We determined the binding to CNGA2 channels in ensemble currents by confocal patch-clamp fluorometry (cPCF) (23, 24). The channels were incorporated in inside-out patches and the fluorescence intensity in the patch dome was measured (Fig. 5A,B). The method provides the advantage to record ligand binding and channel activation in parallel. Both $\mathbf{8}_{G}$ and $\mathbf{10}_{G}$ generated an about ~2.7 fold lower BC_{50} value for CNGA2 channels with respect to $\mathbf{2}_{G}$ (see legend to Fig. 5C).

Brightness of the dye moieties in cGMP derivatives bound to CNGA2 channels

We next tested the brightness of the four fluorescent ligands $\mathbf{2}_G$, $\mathbf{4}_G$, $\mathbf{8}_G$ and $\mathbf{10}_G$ when bound to CNGA2 channels in the excised patches at 10 μ M which is a saturating concentration for all derivatives. To enable comparison at different expression and different patch size, we related the fluorescence of $\mathbf{4}_G$, $\mathbf{8}_G$ and $\mathbf{10}_G$ to that of $\mathbf{2}_G$, the derivative used in our previous studies (23, 25) (Fig. 5D). Notably, $\mathbf{8}_G$ and $\mathbf{10}_G$ if bound to a channel are ~2.0 and ~1.5 times brighter than $\mathbf{2}_G$. Figure 5E shows for the five patches used in Fig. 5D the respective individual bar graphs, here for the photons per pixel. Because the signal is limited by Poisson noise, this doubling of photons corresponds to an increase of the signal-to-noise ratio of $\sqrt{2}$. When plotting the BC_{50} versus the EC_{50} values, there is a positive correlation between the two parameters among the four derivatives as expected (Fig 5F). However, the BC_{50} values increase with a slope bigger than unity at larger EC_{50} values, indicative of a differences in the cooperativity for the ligand binding and activation gating.

The novel fluorescent cAMP derivatives also enhance activation of related HCN2 channels

We previously showed that fcAMP ($\mathbf{2}_A$) activates homologue HCN2 channels similar to the physiological agonist cAMP ($\mathbf{1}_A$) and that the fluorescent derivative can be used to study ligand binding and activation gating in these channels in macropatches by using cPCF (24, 38). To test whether our new fluorescent 8-substituted cAMP derivatives exert a similar effect on HCN2 channels, we activated the channels by a hyperpolarizing voltage pulse (Fig. 6A, top) and, after recording a control current, applied the cAMP derivative $\mathbf{3}_A$, $\mathbf{8}_A$, $\mathbf{9}_A$, $\mathbf{10}_A$ or $\mathbf{11}_A$ at the presumably saturating concentration of 10 μ M (Fig. 6A, bottom). All tested cAMP derivatives enhanced the current amplitude and the speed of

activation as typical for the physiological agonist cAMP (Fig. 6B). For $\mathbf{8}_A$ full concentration-binding relationships were also determined for both closed channels and activated channels at the voltage of -30 mV and -130 mV, respectively (Fig. 6C). Compared to $\mathbf{2}_A$ (2) the relationships at both voltages were shifted by a factor of ~2.5 to lower concentrations, suggesting that the higher potency with $\mathbf{8}_A$ compared to $\mathbf{2}_A$ is caused predominantly by an enhanced binding affinity. Together these results show that the novel compounds are also efficient fluorescent agonists for HCN2 channels.

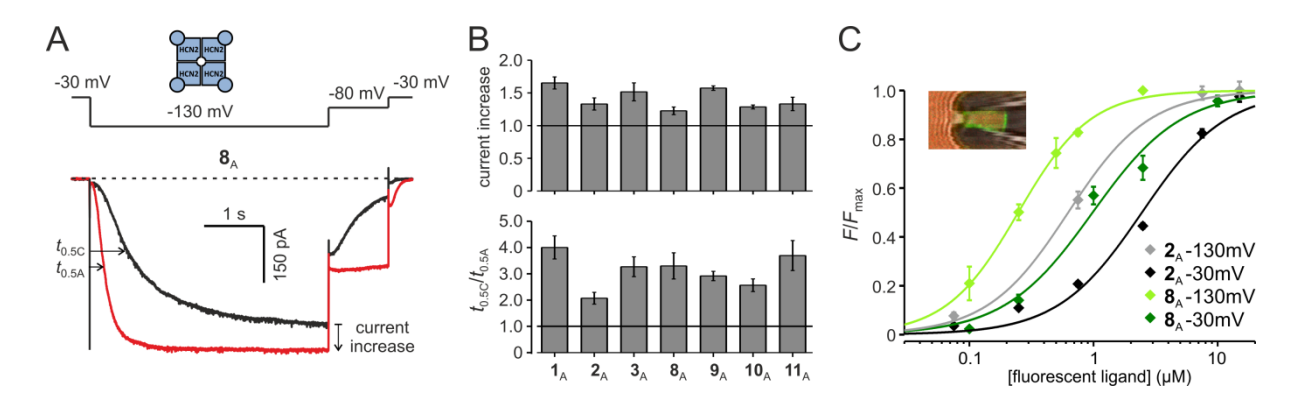


Figure 6. Activation of HCN2 channels by fluorescent cAMP derivatives. (*A*) Voltage protocol and individual current trace in the absence (black) and presence of $\mathbf{8}_{A}$ (red). (*B*) Enhancement of current amplitude (top) and activation speed (bottom) specified by the time interval between hyperpolarizing voltage step and half maximum activation ($t_{0.5}$) by the indicated fluorescent cAMP derivatives. (*C*) Concentration-binding relationship at -30 mV and -130 mV for $\mathbf{8}_{A}$ with respect to $\mathbf{2}_{A}$ as obtained from (2). The curves were obtained by fitting equation 2 to the data points, yielding for $\mathbf{8}_{A}$ -30 mV: BC_{50} =0.98 μM and H_{b} =1.22; $\mathbf{8}_{A}$ -130 mV: BC_{50} =0.25 μM and H_{b} =1.50; $\mathbf{2}_{A}$ -30 mV: BC_{50} =2.46 μM and H_{b} =1.28, and $\mathbf{2}_{A}$ -130 mV: BC_{50} =0.63 μM and H_{b} =1.33.

Discussion

In a combined approach of chemical syntheses and functional tests we synthesized and tested 18 novel fluorescent cyclic nucleotide derivatives capable to activate CNGA2, CNGA2:CNGA4:CNGB1b and HCN2 channels and read out at the same time the amount of ligand binding by confocal patch-clamp fluorometry. With one exception these derivatives are full agonists and, notably, their potency is either similar or significantly enhanced compared to the natural ligands cGMP or cAMP.

Comparison with other fluorescent ligands

In addition to the two DY547 derivatives $\mathbf{2}_G$ (23) and $\mathbf{2}_A$ (24) introduced by our group earlier, the derivative $\mathbf{8}_G$ produced approximately double the brightness (Fig. 5D). Although this increase of brightness seems to be only moderate, it can lead to significant advantages in measurements, because the resolution of the fluorescence signal of the bound ligand is limited by photon-counting (Poisson) noise and the standard deviation of the measurement is proportional to the square root of the number of photons detected. For example, when studying the kinetics of ligand binding by cPCF, doubling of the molecular brightness allows for a two-fold sampling rate or, at the same sampling rate, only half of the expression is required to obtain a similar signal-to-noise ratio. Moreover, experiments on the kinetics of single-ligand binding would profit from a doubled brightness, because the signal-to-noise ratio is improved by the square root of two.

In the past, two other fluorescent derivatives of cyclic nucleotides have been applied to CNG or HCN

channels. In HCN2 channels the cAMP derivative 8-NBD-cAMP has been used to relate ligand binding to channel activation (18). 8-NBD-cAMP produces significantly more fluorescence in the hydrophobic environment of the cyclic nucleotide binding pocket, whereas there is only weak fluorescence in an aqueous environment which therefore does not require confocal recording. Compared to NBD-coupled cyclic nucleotides our DY547- and Cy3B-coupled cyclic nucleotides are advantageous for three reasons: (a) The absorption maximum of Cy3B is at the longer wave length of 559 nm compared to 463 nm for NBD. Therefore, proper excitation can be performed with the 543 nm laser line instead of the 458 nm laser line for NBD, which decreases disturbing autofluorescence and phototoxicity. (b) The brightness, roughly estimated by the product of extinction coefficient and quantum yield, is about ten times higher for Cy3B than for NBD. (c) The bleaching of Cy3B and DY547 is only slow compared to NBD. Moreover, the fluorescent cGMP derivative 8-Fluo-cGMP, containing fluorescein as fluorophore, has been shown already three decades ago to substantially increase the apparent affinity in channels of the rod photoreceptor (17). In our hands, however, this compound is not applicable for optical recording because its illumination in situ rapidly leads to irreversible channel activation. Together, the new compounds tested herein, in particular those with the Cy3B and DY547 dye, are highly appropriate fluorescent and fully functional ligands to activate homo- and heterotetrameric CNG channels as well as HCN2 channels.

Docking of 8_G on the CNBD of CNGA2 channels

It is remarkable that all of our 21 derivatives preserved the activity of the cyclic nucleotide moiety to activate CNG or HCN channels and, moreover, that most of them generated an even increased apparent affinity. What is the structural basis for these results? To address this question, we performed molecular docking for 8_G to the CNBD of CNGA2 channels. The CNGA2 structure was obtained by homology modeling using the TAX-4 structure as a template (1) (see Materials and Methods; Fig. 7A,B). Our computations revealed that the major interactions of the purine system (hydrogen bond with K582) and the phosphate with the CNBD are preserved (hydrogen bonds with I524, R538, T539; c.f. Fig. 7B and Table S3), which is not unexpected because our derivatives preserve the property of being agonists. One surprising difference, however, is that the cGMP derivative was predicted to be in the anti conformation whereas cGMP itself was found in both TAX-4 and HCN channels in the syn conformation (1, 12). A wide groove beside the binding pocket provides the required space for the linker and dye moiety. According to our previous results, also in fluorescent derivatives the hexyl linker might contribute to increased affinity compared to the ethyl linker in that the loss of configurational entropy upon binding is smaller for the hexyl linker (26). Note, however, that fluorophores are bulky substituents, which already might reduce the amount of configurational entropy of the unbound ligand. Therefore, the previously observed complex enthalpy-entropy compensation would be less pronounced for short linkers, which may explain why the apparent higher affinities of ligands with pure short linkers compared to those with longer linkers were not achieved here. Yet, for some of the derivatives with longer linkers, the effect was preserved (e.g., for heterotetramers: 0.23 µM for (Ac)AHT-cGMP versus $0.21 \mu M$ for 3_G ; $0.47 \mu M$ for (Ac)ADT-cAMP versus $0.51 \mu M$ for $9_A(26)$). Another reason may be that the fluorophores interact differently with the protein depending on the linker length, as suggested by the correlation between the Hill coefficient and the linker-length in Figure 4A.

Structural overlay of the CNGA2 and HCN2 CNBDs

In order to understand why the derivatives studied herein are still effective in both CNG and HCN channels, we superimposed the structures of the CNBDs of CNGA2 and HCN2. As expected, the

structures are largely similar (Fig. 7C). But nevertheless we could not reach the high apparent affinities of cAMP (28.8 nM) or even (Ac)ADT-cAMP (14.6 nM) on HCN2 channels (26). Notably, there are also three other proteins with similarly structured CNBDs but entirely different function: protein kinase A, exchange protein directly activated by cAMP (Epac) and the prokaryotic cAMP receptor CAP (39, 40). The effects of cyclic nucleotides on these proteins have been intensively studied previously (41-45). It seems to be an attractive idea to test our set of fluorescent cyclic nucleotide derivatives also on these proteins to learn more about the biophysics of the binding process there.

Furthermore, a test strategy using different dyes and linkers could be beneficial also for other ligandactivated receptors to find and characterize optimal fluorescent compounds.

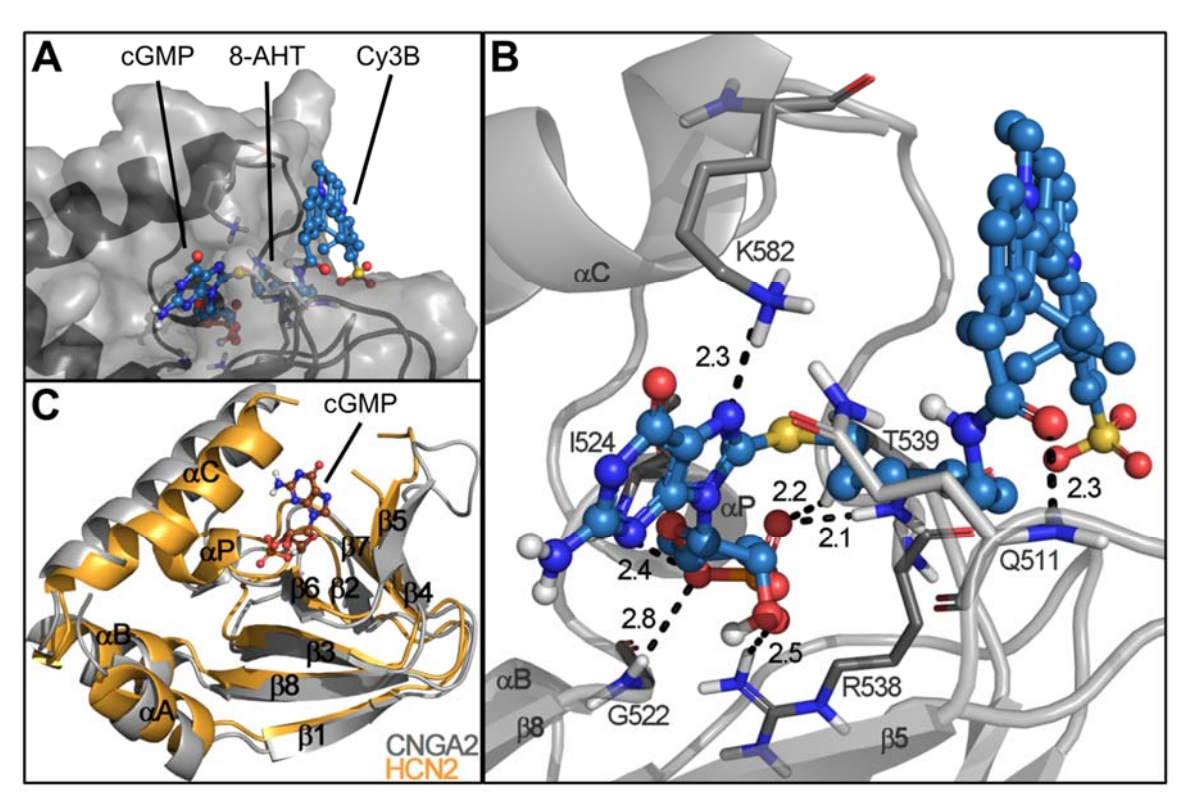


Figure 7. Docking of 8_G to the CNBD in rat CNGA2 channels. (A) Surface representation (grey). Dark grey: α-helices and β-sheets. Atoms in 8_G : blue: carbon; red: oxygen; dark blue: nitrogen; yellow: sulfur; orange: phosphorous. The cyclic nucleotide moiety of 8_G is located in its usual position in the CNBD. The Cy3B moiety and the connecting linker are directed to the outside, thereby filling a groove of the channel structure where they have enough space. (B) Interaction map. Hydrogen bonds and distances are indicated by black dashed lines and numbers [Å], respectively. The phosphate moiety of cGMP interacts with the CNBD in a similar manner as described for TAX-4 channels (1) while the Cy3B moiety nestles up to the outer surface of the channel. (C) Superimposition of the CNBDs of rat CNGA2 (grey) and mouse HCN2 (orange; PDB ID 1Q3E) with cGMP. The structures are very similar.

Differences between cGMP and cAMP derivatives in the apparent affinity with CNG channels

The cGMP derivatives are more potent with homotetrameric CNGA2 than with natural heterotetrameric CNGA2:CNGA4:CNGB1b channels (Fig. 3). These findings are in contrast to the cAMP derivatives which show a higher affinity to heterotetrameric channels. Note again that cAMP is the endogenous ligand for these channels. For understanding the function of the whole channel more thoroughly, it is desirable to follow the gating mechanism of each single subunit in the context of its interaction with the other subunits. With the novel fluorescent cAMP derivatives we provide promising tools to also investigate in a better manner the binding of the less affine CNGA2 subunits in heterotetrameric channels, e.g. by disabling the binding sites of the CNGA4 and CNGB1b subunit with appropriate mutations.

Outlook

The derivatives with the highest affinity (lowest EC_{50} ; c.f. Fig. 1) for the specific channel and reasonable brightness bear potential to relating ligand binding to the activation in single channels by combining optical with electrical recording (46). Such measurements will open a new window to learn how the binding and unbinding events are related to the activation and deactivation gating of single functional channels.

References

- 1. Li, M., X. Zhou, S. Wang, I. Michailidis, Y. Gong, D. Su, H. Li, X. Li, and J. Yang. 2017. Structure of a eukaryotic cyclic-nucleotide-gated channel. Nature 542:60-65.
- 2. Thon, S., E. Schulz, J. Kusch, and K. Benndorf. 2015. Conformational Flip of Nonactivated HCN2 Channel Subunits Evoked by Cyclic Nucleotides. Biophys J 109:2268-2276.
- 3. Kaupp, U. B., and R. Seifert. 2002. Cyclic Nucleotide-Gated Ion Channels. Physiol Rev 82:769-824.
- 4. Matulef, K., and W. N. Zagotta. 2003. Cyclic nucleotide-gated ion channels. Annu Rev Cell Dev Biol 19:23-44.
- 5. Yu, F. H., V. Yarov-Yarovoy, G. A. Gutman, and W. A. Catterall. 2005. Overview of molecular relationships in the voltage-gated ion channel superfamily. Pharmacol Rev 57:387-395.
- 6. Nache, V., N. Wongsamitkul, J. Kusch, T. Zimmer, F. Schwede, and K. Benndorf. 2016. Deciphering the function of the CNGB1b subunit in olfactory CNG channels. Sci Rep 6:29378.
- 7. Nache, V., T. Zimmer, N. Wongsamitkul, R. Schmauder, J. Kusch, L. Reinhardt, W. Bonigk, R. Seifert, C. Biskup, F. Schwede, and K. Benndorf. 2012. Differential regulation by cyclic nucleotides of the CNGA4 and CNGB1b subunits in olfactory cyclic nucleotide-gated channels. Sci Signal 5:ra48.

- 8. Ludwig, A., X. Zong, J. Stieber, R. Hullin, F. Hofmann, and M. Biel. 1999. Two pacemaker channels from human heart with profoundly different activation kinetics. EMBO J 18:2323-2329.
- 9. Ludwig, A., X. Zong, M. Jeglitsch, F. Hofmann, and M. Biel. 1998. A family of hyperpolarization-activated mammalian cation channels. Nature 393:587-591.
- 10. Lee, C. H., and R. MacKinnon. 2017. Structures of the Human HCN1 Hyperpolarization-Activated Channel. Cell 168:111-120 e111.
- 11. Xu, X., Z. V. Vysotskaya, Q. Liu, and L. Zhou. 2010. Structural basis for the cAMP-dependent gating in the human HCN4 channel. The Journal of biological chemistry 285:37082-37091.
- 12. Zagotta, W. N., N. B. Olivier, K. D. Black, E. C. Young, R. Olson, and E. Gouaux. 2003. Structural basis for modulation and agonist specificity of HCN pacemaker channels. Nature 425:200-205.
- 13. Lolicato, M., M. Nardini, S. Gazzarrini, S. Moller, D. Bertinetti, F. W. Herberg, M. Bolognesi, H. Martin, M. Fasolini, J. A. Bertrand, C. Arrigoni, G. Thiel, and A. Moroni. 2011. Tetramerization dynamics of C-terminal domain underlies isoform-specific cAMP gating in hyperpolarization-activated cyclic nucleotide-gated channels. J Biol Chem 286:44811-44820.
- 14. Biel, M., C. Wahl-Schott, S. Michalakis, and X. Zong. 2009. Hyperpolarization-activated cation channels: from genes to function. Physiol Rev 89:847-885.
- 15. Brown, R. L., T. Strassmaier, J. D. Brady, and J. W. Karpen. 2006. The pharmacology of cyclic nucleotide-gated channels: emerging from the darkness. Curr Pharm Des 12:3597-3613.
- 16. Strassmaier, T., and J. W. Karpen. 2007. Novel N7- and N1-substituted cGMP derivatives are potent activators of cyclic nucleotide-gated channels. Journal of medicinal chemistry 50:4186-4194.
- 17. Tanaka, J. C., J. F. Eccleston, and R. E. Furman. 1989. Photoreceptor channel activation by nucleotide derivatives. Biochemistry 28:2776-2784.
- 18. Wu, S., Z. V. Vysotskaya, X. Xu, C. Xie, Q. Liu, and L. Zhou. 2011. State-dependent cAMP binding to functioning HCN channels studied by patch-clamp fluorometry. Biophys J 100:1226-1232.
- 19. Bois, P., B. Renaudon, M. Baruscotti, J. Lenfant, and D. DiFrancesco. 1997. Activation of f-channels by cAMP analogues in macropatches from rabbit sino-atrial node myocytes. J Physiol 501 (Pt 3):565-571.
- 20. Moller, S., A. Alfieri, D. Bertinetti, M. Aquila, F. Schwede, M. Lolicato, H. Rehmann, A. Moroni, and F. W. Herberg. 2014. Cyclic nucleotide mapping of hyperpolarization-activated cyclic nucleotide-gated (HCN) channels. ACS Chem Biol 9:1128-1137.
- 21. Scott, S. P., P. W. Shea, and S. E. Dryer. 2007. Mapping ligand interactions with the hyperpolarization activated cyclic nucleotide modulated (HCN) ion channel binding domain using a soluble construct. Biochemistry 46:9417-9431.
- 22. Caretta, A., A. Cavaggioni, and R. T. Sorbi. 1985. Binding stoichiometry of a fluorescent cGMP analogue to membranes of retinal rod outer segments. European journal of biochemistry / FEBS 153:49-53.
- 23. Biskup, C., J. Kusch, E. Schulz, V. Nache, F. Schwede, F. Lehmann, V. Hagen, and K. Benndorf. 2007. Relating ligand binding to activation gating in CNGA2 channels. Nature 446:440-443.
- 24. Kusch, J., C. Biskup, S. Thon, E. Schulz, V. Nache, T. Zimmer, F. Schwede, and K. Benndorf. 2010. Interdependence of receptor activation and ligand binding in HCN2 pacemaker channels. Neuron 67:75-85.
- 25. Nache, V., T. Eick, E. Schulz, R. Schmauder, and K. Benndorf. 2013. Hysteresis of ligand binding in CNGA2 ion channels. Nature communications 4:2864.
- 26. Otte, M., A. Schweinitz, M. Bonus, U. Enke, C. Schumann, H. Gohlke, and K. Benndorf. 2018. Hydrophobic alkyl chains substituted to the 8-position of cyclic nucleotides enhance activation of CNG and HCN channels by an intricate enthalpy entropy compensation. Sci Rep 8:14960.
- 27. Hamill, O. P., A. Marty, E. Neher, B. Sakmann, and F. J. Sigworth. 1981. Improved patch-clamp techniques for high-resolution current recording from cells and cell-free membrane patches. Pflugers Arch 391:85-100.
- 28. DiFrancesco, D. 1986. Characterization of single pacemaker channels in cardiac sino-atrial node cells. Nature 324:470-473.

- 29. Biasini, M., S. Bienert, A. Waterhouse, K. Arnold, G. Studer, T. Schmidt, F. Kiefer, T. Gallo Cassarino, M. Bertoni, L. Bordoli, and T. Schwede. 2014. SWISS-MODEL: modelling protein tertiary and quaternary structure using evolutionary information. Nucleic Acids Res 42:W252-258.
- 30. Chen, V. B., W. B. Arendall, 3rd, J. J. Headd, D. A. Keedy, R. M. Immormino, G. J. Kapral, L. W. Murray, J. S. Richardson, and D. C. Richardson. 2010. MolProbity: all-atom structure validation for macromolecular crystallography. Acta Crystallogr D Biol Crystallogr 66:12-21.
- 31. Frisch, M. J., G.W. Trucks, H.B. Schlegel, G.E. Scuseria, M.A. Robb, J.R. Cheeseman, G. Scalmani, V. Barone, B. Mennucci, G.A. Petersson, H. Nakatsuji, M. Caricato, X. Li, H.P. Hratchian, A.F. Izmaylov, J. Bloino, G. Zheng, J.L. Sonnenberg, M. Hada, M. Ehara, K. Toyota, R. Fukuda, J. Hasegawa, M. Ishida, T. Nakajima, Y. Honda, O. Kitao, H. Nakai, T. Vreven, J.A. Montgomery, J.E. Peralta, F. Ogliaro, M. Bearpark, J.J. Heyd, E. Brothers, K.N. Kudin, V.N. Staroverov, R. Kobayashi, J. Normand, K. Raghavachari, A. Rendell, J.C. Burant, S.S. Iyengar, J. Tomasi, M. Cossi, N. Rega, J.M. Millam, M. Klene, J.E. Knox, J.B. Cross, V. Bakken, C. Adamo, J. Jaramillo, R. Gomperts, R.E. Stratmann, O. Yazyev, A.J. Austin, R. Cammi, C. Pomelli, J.W. Ochterski, R.L. Martin, K. Morokuma, V.G. Zakrzewski, G.A. Voth, P. Salvador, J.J. Dannenberg, S. Dapprich, A.D. Daniels, Farkas, J.B. Foresman, J.V. Ortiz, J. Cioslowski, D.J. Fox 2009. Gaussian 09, Revision B.01. In Wallingford CT.
- 32. Vanquelef, E., S. Simon, G. Marquant, E. Garcia, G. Klimerak, J. C. Delepine, P. Cieplak, and F. Y. Dupradeau. 2011. R.E.D. Server: a web service for deriving RESP and ESP charges and building force field libraries for new molecules and molecular fragments. Nucleic Acids Res 39:W511-517.
- 33. Wang, J. M., P. Cieplak, and P. A. Kollman. 2000. How well does a restrained electrostatic potential (RESP) model perform in calculating conformational energies of organic and biological molecules? Journal of Computational Chemistry 21:1049-1074.
- 34. Hornak, V., R. Abel, A. Okur, B. Strockbine, A. Roitberg, and C. Simmerling. 2006. Comparison of multiple Amber force fields and development of improved protein backbone parameters. Proteins 65:712-725.
- 35. Cornell, W. D., P. Cieplak, C. I. Bayly, I. R. Gould, K. M. Merz, D. M. Ferguson, D. C. Spellmeyer, T. Fox, J. W. Caldwell, and P. A. Kollman. 1995. A 2nd Generation Force-Field for the Simulation of Proteins, Nucleic-Acids, and Organic-Molecules. Journal of the American Chemical Society 117:5179-5197.
- 36. Morris, G. M., D. S. Goodsell, R. Huey, and A. J. Olson. 1996. Distributed automated docking of flexible ligands to proteins: parallel applications of AutoDock 2.4. J Comput Aided Mol Des 10:293-304.
- 37. Brown, R. L., R. J. Bert, F. E. Evans, and J. W. Karpen. 1993. Activation of retinal rod cGMP-gated channels: what makes for an effective 8-substituted derivative of cGMP? Biochemistry 32:10089-10095.
- 38. Kusch, J., S. Thon, E. Schulz, C. Biskup, V. Nache, T. Zimmer, R. Seifert, F. Schwede, and K. Benndorf. 2012. How subunits cooperate in cAMP-induced activation of homotetrameric HCN2 channels. Nat Chem Biol 8:162-169.
- 39. Dremier, S., R. Kopperud, S. O. Doskeland, J. E. Dumont, and C. Maenhaut. 2003. Search for new cyclic AMP-binding proteins. FEBS Lett 546:103-107.
- 40. Bos, J. L. 2006. Epac proteins: multi-purpose cAMP targets. Trends Biochem Sci 31:680-686.
- 41. Berman, H. M., L. F. Ten Eyck, D. S. Goodsell, N. M. Haste, A. Kornev, and S. S. Taylor. 2005. The cAMP binding domain: an ancient signaling module. Proc Natl Acad Sci U S A 102:45-50.
- 42. Akimoto, M., R. Selvaratnam, E. T. McNicholl, G. Verma, S. S. Taylor, and G. Melacini. 2013. Signaling through dynamic linkers as revealed by PKA. Proc Natl Acad Sci U S A 110:14231-14236.
- 43. Popovych, N., S. R. Tzeng, M. Tonelli, R. H. Ebright, and C. G. Kalodimos. 2009. Structural basis for cAMP-mediated allosteric control of the catabolite activator protein. Proc Natl Acad Sci U S A 106:6927-6932.

- 44. Selvaratnam, R., M. T. Mazhab-Jafari, R. Das, and G. Melacini. 2012. The auto-inhibitory role of the EPAC hinge helix as mapped by NMR. PloS one 7:e48707.
- 45. Selvaratnam, R., B. VanSchouwen, F. Fogolari, M. T. Mazhab-Jafari, R. Das, and G. Melacini. 2012. The projection analysis of NMR chemical shifts reveals extended EPAC autoinhibition determinants. Biophys J 102:630-639.
- 46. Schmauder, R., D. Kosanic, R. Hovius, and H. Vogel. 2011. Correlated optical and electrical single-molecule measurements reveal conformational diffusion from ligand binding to channel gating in the nicotinic acetylcholine receptor. Chembiochem 12:2431-2434.

Acknowledgements

We thank K. Schoknecht, S. Bernhardt, A. Kolchmeier and C. Ranke for excellent technical assistance. We are also grateful to Prof. U. Schubert, Institute of Organic Chemistry, Friedrich Schiller University Jena, and to Prof. C. Schumann, Ernst-Abbe-University of Applied Sciences Jena, for providing lab space for chemical syntheses. This project was partly funded by the German Research Foundation (DFG) within the TRR 166 ReceptorLight (project A05) to KB, Research Group FOR 2518 DynIon (projects P2 to KB and P7 to HG), and by the Thüringer Ministerium für Wirtschaft, Wissenschaft und Digitale Gesellschaft, Dag-ION (project 2025-514 to KB). HG is grateful for computational support and infrastructure provided by the "Zentrum für Informations- und Medientechnologie" (ZIM) at the Heinrich Heine University Düsseldorf.

Authorship Contributions

M.O., S.T., and U.E. conducted the patch-clamp recordings, M.O., S.T. and S.Y. conducted the combined electrophysiological and optical experiments. M.O. performed the docking experiments. M.B. and H.G. derived charges for the derivative $\mathbf{8}_G$ for the docking experiments. M.O., S.T., R.S. performed the data analyses. M.L., A.S. and U.E. conducted the chemical syntheses. K.B. and R.S. designed the study. M.O. and S.T prepared the figures. H.G. contributed to the writing of the docking experiments. K.B. wrote the manuscript.

Competing interests

The author(s) declare no competing interests.